Supporting Information

Ag Nanoparticle Embedded Cu Nanoporous Hybrid Arrays for the Selective Electrocatalytic Reduction of CO_2 towards Ethylene

Liang Hou[1 §], Jianyu Han[2 §], Chong Wang[1], Yuwei Zhang[1], Yuanbin Wang[1], Zhiming Bai[3]*, Yousong Gu[1], Yan Gao[2]*, Xiaoqin Yan[1]*

1. School of Materials Science and Engineering, University of Science and Technology Beijing, Beijing 100083, People's Republic of China. E-mail: xqyan@mater.ustb.edu.cn

2. Laboratory of Nanomaterials, National Center for Nanoscience and Technology, Beijing, 100190, People's Republic of China. E-mail: gaoyan@nanoctr.cn

3. School of Civil and Resource Engineering, University of Science and Technology Beijing, Beijing 100083, P. R. China. E-mail: baizhiming2008@126.com

§ These two authors contributed equally.

Table of Contents

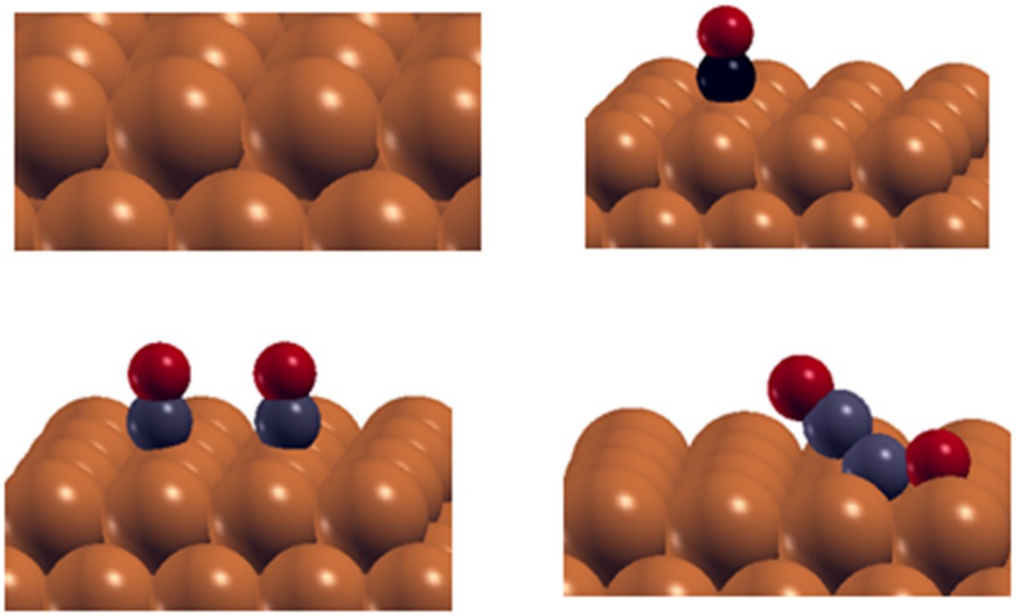

Fig. S1 The optimized geometries of various Cu surfaces for examining the *CO adsorption and CO=CO dimenrization during CO_2RR. Filled circles with orange is Cu, brown is C and red is O.

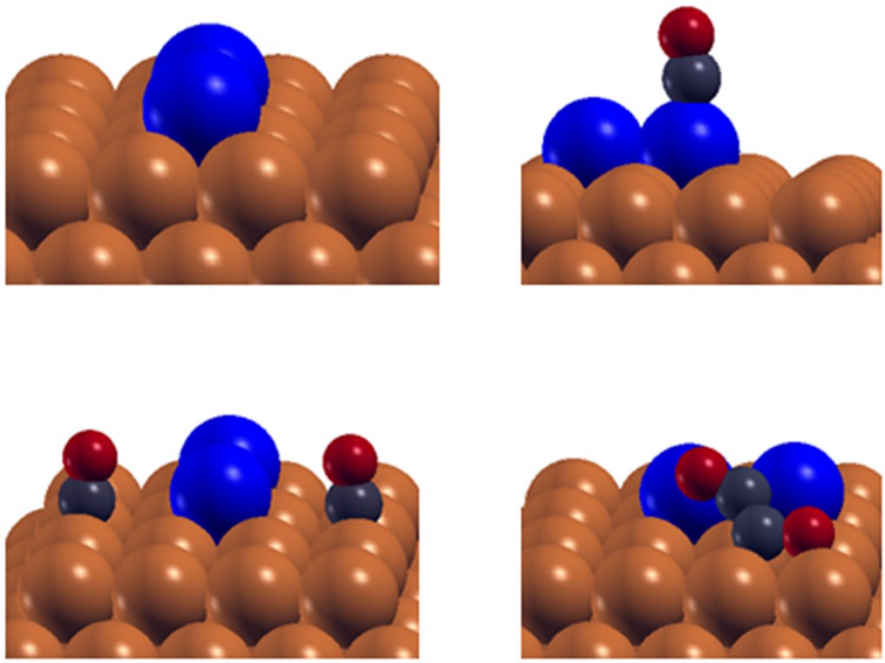

Fig. S2 The optimized geometries of various Ag/Cu surfaces for examining the *CO adsorption and CO=CO dimenrization during CO_2RR. Filled circles with orange is Cu, blue is Ag, brown is C and red is O.

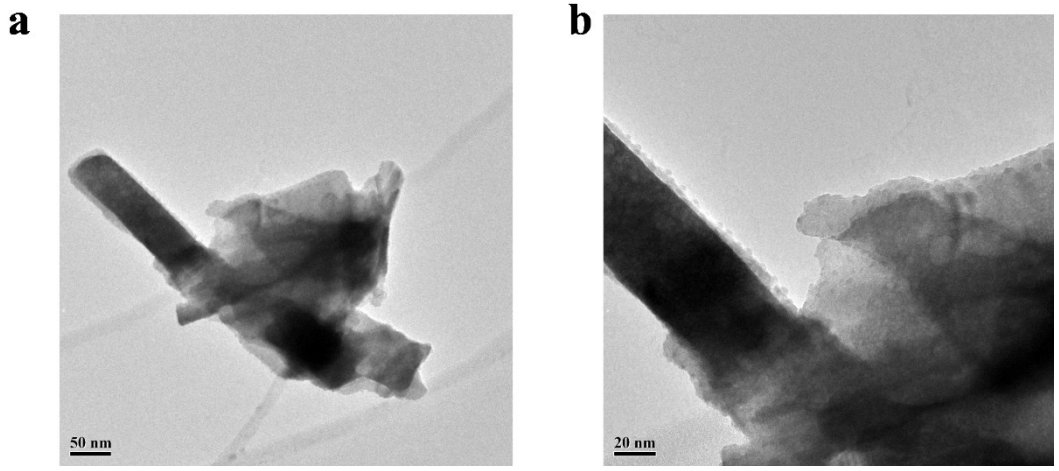

Fig. S3 TEM characterization of Ag@Cu Np hybrid arrays at different magnifications(a) (b).

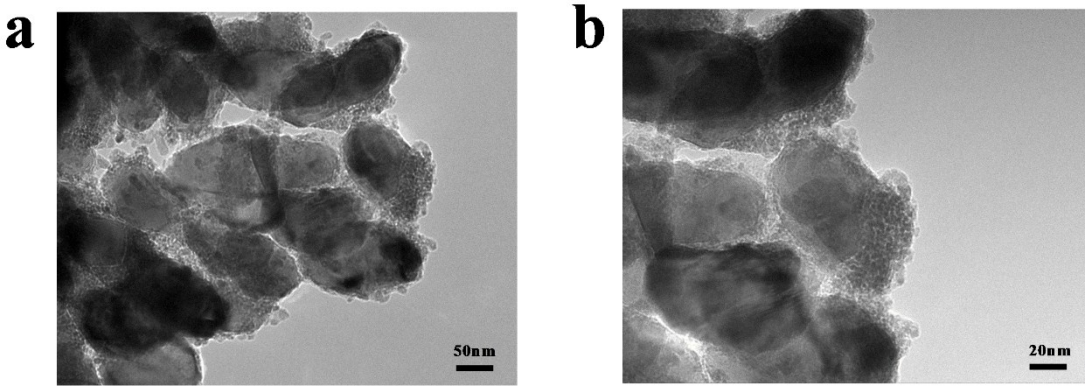

Fig. S4 TEM characterization of Zn@Cu Np hybrid arrays at different magnifications(a) (b).

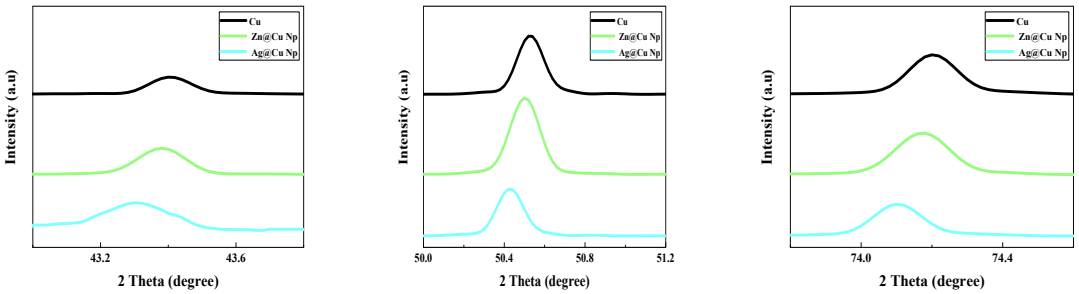

Fig. S5 Enlarged XRD patterns of Cu, Ag@Cu Np, Zn@Cu Np hybrid arrays in the diffraction peaks of (111), (200), and (220) facet.

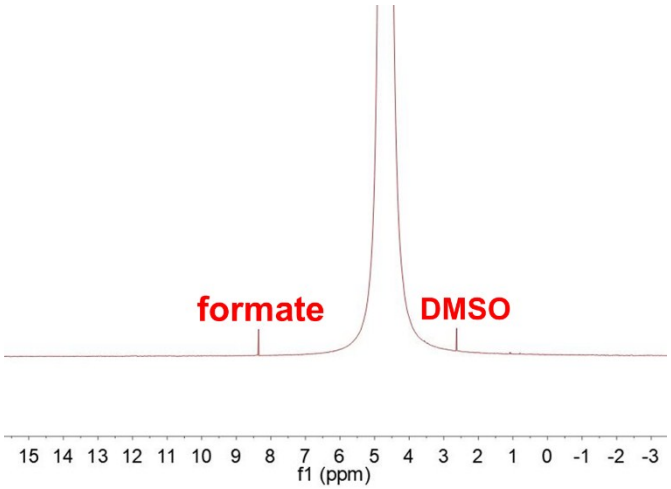

Fig. S6 Representative 1H NMR (400 MHz, D_2O, 298K) of electrocatalytic CO_2 reduction on Ag@Cu Np at -1.2V vs. RHE in 0.5 M $KHCO_3$. DMSO was used as an internal standard for liquid product quantification.

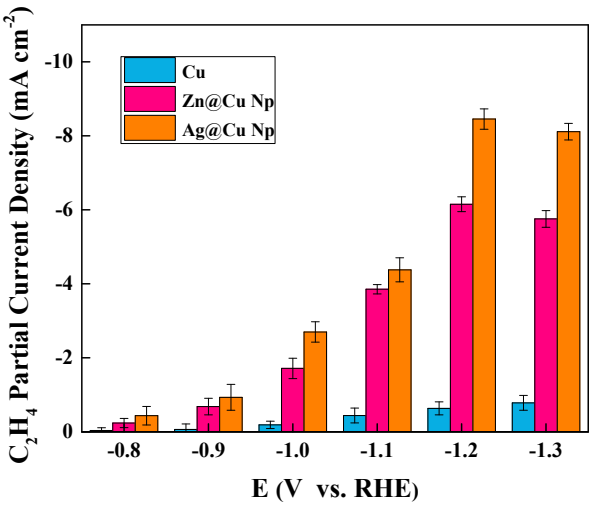

Fig. S7 C_2H_4 partical current density of Ag@Cu Np pre-catalyst (orange), Zn@Cu Np pre-catalyst (dark pink) and Cu pre-catalyst (light blue) in the potential range from -0.8 to -1.2 V (vs. RHE).

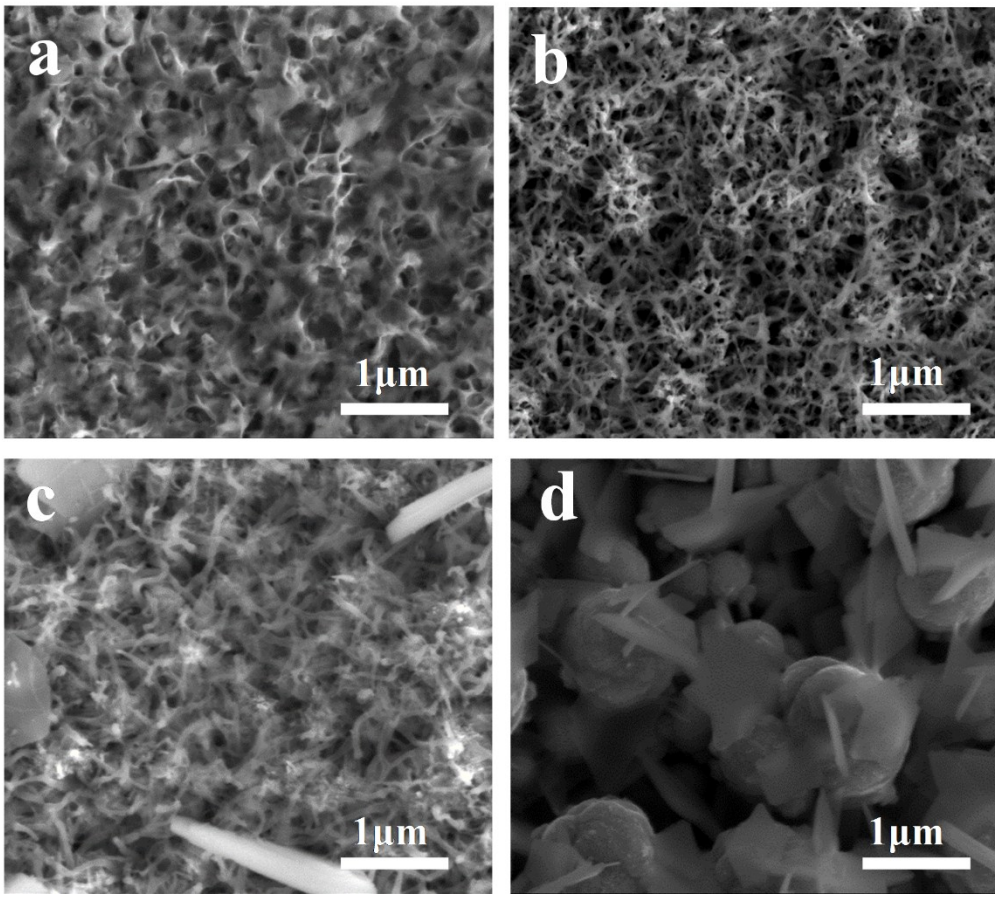

Fig. S8 SEM images of (a) Cu Np, (b)(c)(d) Ag@Cu Np with different Ag contents (2,5,10mmol), respectively.

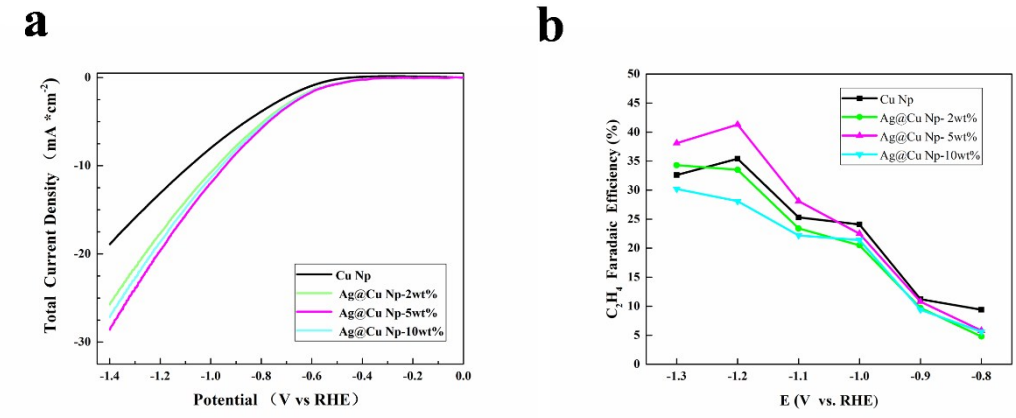

Fig. S9 Electrocatalytic performance of Ag@CuNp with different Ag contents (wt%). (a) LSV curves of Ag@Cu Np with different Ag contents (0%, 2%, 5%, 10%). (b) Ethylene Faradaic efficiencies of Ag@Cu Np pre-catalyst with different Ag contents (0%, 2%, 5%, 10%) in the potential range from -0.8 to -1.3 V (vs. RHE).

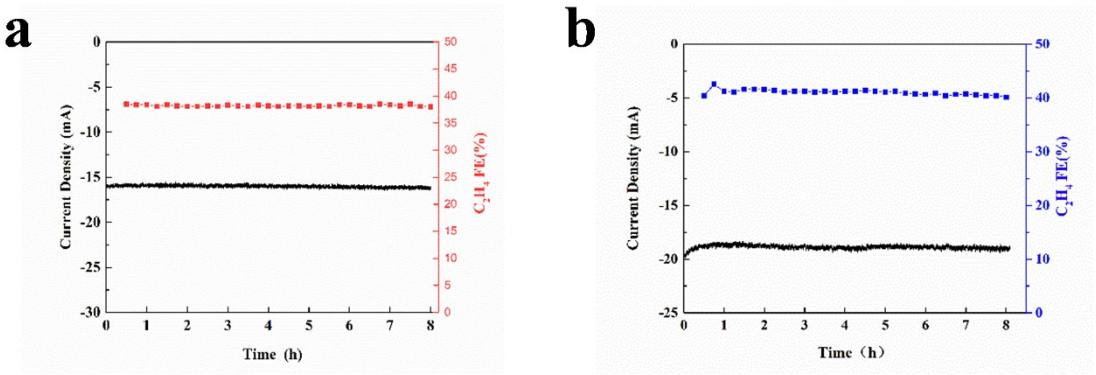

Fig. S10 Long-term stability of Zn@Cu Np(a) and Ag@Cu Np (b) pre-catalysts at a potential load of −1.2V (vs. RHE) and the corresponding Faradaic efficiency of ethylene.

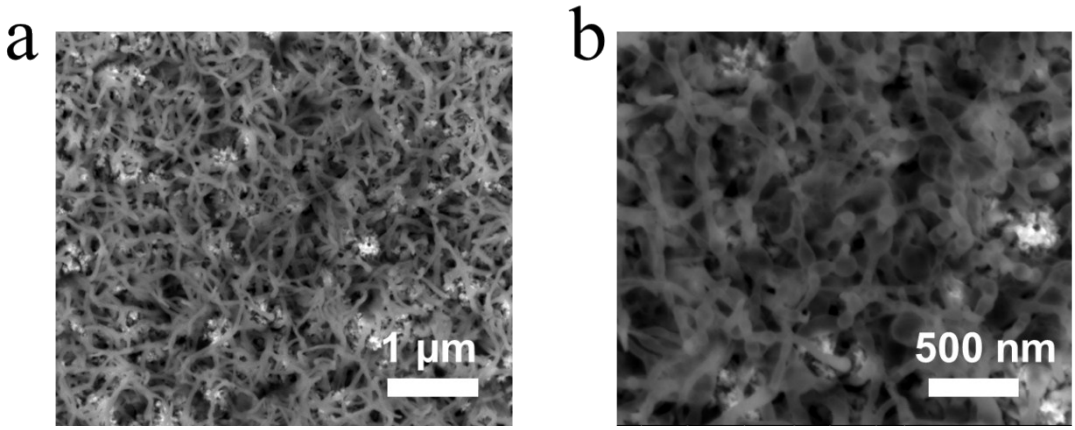

Fig. S11 SEM images of Ag@Cu Np at different magnifications(a) (b) after electrocatalytic CO_2 reduction.

Table. S1 Recently reported highly active catalysts for CO_2 reduction in an aqueous solution.

Catalysts	Electrolyte	Main Product	Potential	F.E.	Ref.
Cu Nanowire Arrays	0.1M $KHCO_3$	C_2H_4	-1.1v	17.4%	S1
Cu Mesoporous	0.1M $KHCO_3$	C_2H_4	-1.3v	38%	S2
Cu nanocubes	0.1M $KHCO_3$	C_2H_4	-1.1v	41%	S3
Phase-separated Cu-Pd	1 M KOH	C_2H_4, C_2H_5OH	—	Total: 63%	S4
B-doped Cu	0.1M $KHCO_3$	C_2H_4, C_2H_5OH	-1.1v	52%and 27%	S5
O_2-plasma-treated Cu	0.1M $KHCO_3$	C_2H_4	-0.9v	60%	S6
Cu_2O films	0.1M $KHCO_3$	C_2H_4, C_2H_5OH	-0.99 v	34 %and16 %	S7
Ag-Cu Nanodimers	0.1M $KHCO_3$	C_2H_4	-1.1v	40%	S8
oxide-derived Cu_XZn	0.1M $KHCO_3$	C_2H_5OH	-1.0v	29.1%	S9
Ag	0.1M $KHCO_3$	CO	-0.5V	90%	S10
Zn	0.1M $KHCO_3$	CO	-0.9v	47.55 %	S11

References

S1 M. Ma, K. Djanashvili and W. A. Smith, Controllable Hydrocarbon Formation from the Electrochemical Reduction of CO_2 over Cu Nanowire Arrays, *Angew. Chem. Int. Ed.*, 2016, **55**, 6680.

S2 K. D. Yang, W. R. Ko, J. H. Lee, S. J. Kim, H. Lee, M. H. Lee and K. T. Nam, Morphology-Directed Selective Production of Ethylene or Ethanefrom CO_2 on a Cu Mesopore Electrode, *Angew. Chem. Int. Ed*., 2017, **56**, 796.

S3 A. Loiudice, P. Lobaccaro, E. A. Kamali, T. Thao, B. H. Huang, J. W. Ager and R. Buonsanti, Tailoring Copper Nanocrystals towards C_2 Products in Electrochemical CO_2 Reduction, *Angew. Chem. Int. Ed.*, 2016, **55**, 5789.

S4 S. Ma, M. Sadakiyo, M. Heima, R. Luo, R. T. Haasch, J. I. Gold, M. Yamauchi and P. J. Kenis, Electroreduction of carbon dioxide to hydrocarbons using bimetallic Cu-Pd catalysts with different mixing patterns, *J. Am. Chem. Soc.*, 2017, **139**, 47.

S5 Y. Zhou, F. Che, M. Liu, C. Zou, Z. Liang, P. De Luna, H. Yuan, J. Li, Z. Wang, H. Xie, H. Li, P. Chen, E. Bladt, R. Quintero-Bermudez, T. K. Sham, S. Bals, J. Hofkens, D. Sinton, G. Chen and E. H. Sargent, Dopant-induced electron localization drives CO_2 reduction to C_2 hydrocarbons, *Nat. Chem*., 2018, **10**, 974.

S6 H. Mistry, A. S. Varela, C. S. Bonifacio, I. Zegkinoglou, I. Sinev, Y. W. Choi, K. Kisslinger, E. A. Stach, J. C. Yang, P. Strasser and B. R. Cuenya, Highly selective

plasma-activated copper catalysts for carbon dioxide reduction to ethylene, *Nat. Commun*., 2016, **7**, 12123.

S7 D. Ren, Y. Deng, A. D. Handoko, C. S. Chen, S. Malkhandi and B. S. Yeo, Selective electrochemical reduction of carbon dioxide to ethylene and ethanol on copper (I) oxide catalysts, *ACS Catal.*, 2015, **5**, 2814.

S8 J. Huang, M. Mensi, E. Oveisi, V. Mantella and R. Buonsanti, Structural Sensitivities in Bimetallic Catalysts for Electrochemical CO_2 Reduction Revealed by Ag-Cu Nanodimers. *J. Am. Chem. Soc.*, 2019, **141**, 2490.

S9 D.Ren, B S H Ang and B S. Yeo, Tuning the selectivity of carbon dioxide electroreduction toward ethanol on oxide-derived Cu_XZn catalysts. *ACS Catal*., 2016, **6**, 8239.

S10 H. Mistry, Y. W. Choi, A. Bagger, F. Scholten, C. S. Bonifacio, I. Sinev, N. J. Divins, I. Zegkinoglou, H. S. Jeon, K. Kisslinger, E. A. Stach, J. C. Yang, J. Rossmeisl, B. Roldan Cuenya, Enhanced carbon dioxide electroreduction to carbon monoxide over defect-rich plasma-activated silver catalysts, *Angew. Chem. Int. Ed*., 2017, **56**, 11394.

S11 B. Qin, Y. Li, H. Fu, H. Wang, S. Chen, Z.Liu and F. Peng, Electrochemical reduction of CO_2 into tunable syngas production by regulating the crystal facets of earth-abundant Zn catalyst. *ACS. Appl. Mater. Inter*, 2018, **10**, 20530.